NASA Technical Memorandum 105938

Experimental Investigation of Cyclic Thermomechanical Deformation in Torsion

Michael G. Castelli
Sverdrup Technology, Inc.
Brook Park, Ohio

Charles E. Bakis
Pennsylvania State University
University Park, Pennsylvania

and

John R. Ellis
Lewis Research Center
Cleveland, Ohio

November 1992

NASA

EXPERIMENTAL INVESTIGATION OF CYCLIC THERMOMECHANICAL DEFORMATION IN TORSION

Michael G. Castelli
Sverdrup Technology, Inc.
Lewis Research Center Group
Brook Park, Ohio 44142

Charles E. Bakis
Department of Engineering Science and Mechanics
The Pennsylvania State University
University Park, Pennsylvania 16802

and

John R. Ellis
National Aeronautics and Space Administration
Lewis Research Center
Cleveland, Ohio 44135

SUMMARY

An investigation of thermomechanical testing and deformation behavior of tubular specimens under torsional loading is described. Experimental issues concerning test accuracy and control specific to thermomechanical loadings under a torsional regime are discussed. A series of shear strain-controlled tests involving the nickel-base superalloy Hastelloy X were performed with various temperature excursions and compared to similar thermomechanical uniaxial tests. The concept and use of second invariants of the deviatoric stress and strain tensors as a means of comparing uniaxial and torsional deformations is presented and critiqued for its applicability to the present data. The hardening behavior of the torsional specimens is also briefly presented and discussed in light of previous thermomechanical tests conducted under uniaxial conditions.

INTRODUCTION

In most high temperature engineering applications, components are subjected to complex combinations of thermal and mechanical loadings during service. Such thermomechanical loadings have long been identified as limiting factors in the design of structural components. In addition, certain structural alloys display unique deformation behaviors under specific thermomechanical paths: behaviors which are not experienced under more commonly investigated isothermal conditions (refs. 1 to 3). This potential for life limiting behavior and unique deformation response under thermomechanical loading is clearly sufficient to warrant careful consideration and investigation.

Despite the demonstrated need for closely controlled thermomechanical deformation (TMD) experiments, such experiments are seldom performed due to numerous experimental complexities introduced (e.g., phasing between the mechanical component of loading and temperature, dynamic temperature gradients, and cyclic temperature control). Many of these issues are further complicated in axial strain-controlled tests in which thermal strains have a first order effect on the test control variable: the specimen's total strain (refs. 1 and 4 to 6). If a specific mechanical strain range is desired, an accurate

account of and compensation for the thermal strain component must be maintained throughout the test. Even with digital test control, this remains a complex task.

One approach to minimize or potentially eliminate the coupling between mechanical and thermal strains is to perform thermomechanical strain-controlled tests under torsion. Under such conditions, the strain in the loading direction (pure shear) is theoretically not affected by temperature excursions. Thus, there is no need to account for thermal strain effects and, as a result, test control is greatly simplified (refs. 7 and 8). Moreover, a torsion test enables the measurement of the entire mechanical strain tensor with a single measurement, whereas two or three measurements are required to measure the full mechanical strain tensor in a uniaxial test. Typically, however, only the strain in the loading direction is measured in a uniaxial test. The transverse strains are dependant upon the temperature and relative amounts of elastic and plastic deformation, and are therefore difficult to predict.

The objectives of this investigation were, first, to develop testing capabilities and investigate testing issues concerning closely controlled TMD experiments in torsion, and second, to make comparisons between uniaxial and torsional TMD based on equivalent effective stresses and strains. The second objective was accomplished by conducting torsional and uniaxial TMD experiments with equivalent effective strain limits based on the second invariant of the deviatoric strain tensor. The effective strain limits were calculated from the first cycle of the uniaxial TMD response and subsequently used to dictate the imposed strain values for the analogous test in torsion. By forcing the second invariant of the deviatoric strain tensors to be identical during the first cycle of deformation, appropriate data comparisons could be made in a second deviatoric stress-strain space. Such comparisons were designed to address the validity of the sole use of this scalar quantity for the purposes of comparing and predicting TMD behavior.

NOMENCLATURE

$a_{ij}, \dot{a}_{ij}$	deviatoric internal stress and stress rate tensors, respectively
f, g, h	material functions in the Robinson model
J_2	second invariant of the deviatoric stress tensor
J_2'	second invariant of the deviatoric mechanical strain tensor
$\tilde{J}_2, \hat{J}_2$	second invariant of the effective deviatoric stress tensor and deviatoric internal stress tensor, respectively
K	material parameter in the Robinson model
l, l_0	total and initial axial gage length, respectively
$\Delta l_T, \Delta l_R$	changes in axial gage length resulting from thermal and ratchetting strains, respectively
r_0	original mean radius of specimen
r_i, r, r_{ou}	inner, mean, and outer radius of specimen, respectively
$\Delta r_T, \Delta r_R$	change in mean radius of specimen resulting from thermal and ratchetting strains, respectively
S_{ij}	deviatoric stress tensor

$\tilde{s}_m$	actual lateral displacement resulting from mechanical load
s^*	lateral displacement at mean test temperature resulting from initial indentation misalignment
s	lateral displacement measured by extensometer
s_{i0}	initial indentation misalignment at room temperature
s_i	lateral displacement resulting from indentation misalignment
s_m	measured lateral displacement resulting from mechanical load
$T, \Delta T$	temperature and temperature change, respectively
T_m	mean test temperature
T_{RT}	room temperature
α	linear coefficient of thermal expansion
α_{ij}	internal stress tensor
γ	total engineering shear strain
γ'	desired total engineering shear strain (error calculation)
γ_m, γ_i	engineering shear strain resulting from mechanical load and misalignment, respectively
δ_{ij}	Kronecker delta
$\varepsilon^{el}, \varepsilon^{pl}$	elastic and plastic strains axial strain components, respectively
$\epsilon_{LR}, \epsilon_{HR}$	ratchetting strains in longitudinal and hoop directions, respectively
$\dot{\varepsilon}_{ij}^{in}$	inelastic strain rate tensor
ν^{el}, ν^{pl}	elastic and fully plastic Poisson's ratios, respectively
θ_f, θ_g	material functions (Arrhenius forms) in the Robinson model
ρ	material function in the Robinson model
Σ_{ij}	effective deviatoric stress tensor
σ_{ij}	total stress tensor
T	torque
τ	shear stress
ϕ	total angle of twist in gage length
ϕ_i	angle of initial twist in gage length resulting from initial indentation misalignment

ϕ_m angle of mechanical twist in gage length

Ω complementary dissipation potential

EXPERIMENTAL DETAILS

Test Specimens

The material used for this study was Hastelloy X*—a nickel-base solid-solution-strengthened alloy commonly used in high temperature power generation applications. The torsional and uniaxial specimens were fabricated from separate heats of material. All of the material used in this investigation was produced in accordance with Aerospace Material Specification 5754H and was solution heat treated. The chemical compositions of each heat are shown in table I.

The test specimen geometries are shown in figure 1. Smooth shank ends were used to allow gripping with hydraulically-actuated collet grips. Earlier investigations with both geometries (refs. 4 and 9) have shown the specimens to be well suited for axial and torsional deformation studies on monolithic materials.

Torsional Test Apparatus

All experiments were conducted in an air environment. Heating was provided by an audio frequency induction heater outfitted with the coil fixture partially shown in figure 2 and described completely in reference 10. This fixture supports three coil segments which are independently adjustable in the transverse and axial directions. The three coil segments were wired in series, thereby enabling the use of a single, closed-loop temperature controller. Since no forced cooling was employed, conduction through the water-cooled grips served as the major mechanism for specimen cooling. An enclosure was used around the test frame to minimize the effects of air currents.

A triangular waveform was used for both shear strain and temperature control. This allowed a constant shear strain rate to be maintained throughout the cycle. Cycle periods were dictated by the ability to cycle the specimen's temperature and maintain close control over the desired waveform. This resulted in a 4-min cycle period. The uniaxial TMD tests used for comparison in this study were conducted with an 8-min cycle period due to limitations related to accurate thermal strain compensation (refs. 1 and 4). Such limitations did not arise in the torsional TMD experiments as no thermal strain compensation was required. Previous work on Hastelloy X indicated that a factor of two difference in strain rates should have a negligible effect on the material's deformation response in the temperatures of interest (refs. 1 and 11). Therefore, in an effort to expedite testing, the torsional cycle times were maintained at 4 min. Load in the axial direction was maintained at zero in load control. Shear stress in the gage length was assumed nearly constant through the wall thickness and, as such, was based upon the mean radius (r) in the following manner:

*Hastelloy X is a trademark of Haynes International, Inc., Kokomo, IN.

$$\tau = \frac{2Tr}{\pi\left(r_{ou}^4 - r_i^4\right)} \tag{1}$$

where T is the torque, r_{ou} is the outer radius, and r_i is the inner radius. This approximation is considered reasonable since the mean radius is six times the wall thickness.

The temperature and shear strain waveforms were time-phased with a value of either 0° (in-phase) or 180° (out-of-phase). Therefore, given that all the tests were initiated at the mean temperature of the temperature range, the in-phase (IP) and out-of-phase (OP) torsional tests corresponded to the cases of initial temperature increase and decrease, respectively. For example, an IP test with a temperature range of 400 to 600 °C would initiate at 500 °C and begin loading with temperature increasing towards 600 °C. The corresponding OP test would initiate at 500 °C and begin loading with temperature decreasing towards 400 °C. Note that the mechanical effects of positive or negative strain are identical in pure shear-type loading and the sign is strictly an issue of convention. Thus, the difference between IP and OP deformation in this study rests exclusively on the condition of initially loading towards the hot extreme of the temperature range (IP) or the cold extreme of the temperature range (OP). This is not the case for the uniaxial TMD experiments where IP or OP implies that the maximum temperature coincides with the maximum tensile or compressive mechanical strain, respectively (ref. 4).

A minicomputer was used to command the temperature and shear strain control signals. Temperature, torque, axial strain and shear strain were digitally recorded at a rate of one sample point per second (with each sample point representing the average of 100 measurements over the previous second). Axial and shear strains were measured with a water-cooled extensometer utilizing quartz probes with a gage length of 25 mm. The probes were spring-loaded against indents of 250 μm nominal depth indented on the outside diameter of the specimen (figs. 2 and 3). The extensometer provided an output which was proportional to the lateral displacement (s) of the lower probe relative to the upper probe. It was assumed that $s = r\phi_m$, where r is the mean radius and ϕ_m is the angle of twist in the gage length. The shear strain, γ, was then calculated as follows:

$$\gamma = \frac{s}{l_0} \tag{2}$$

where l_0 is the nominal gage length of the extensometer (25 mm). Additional details of the axial/torsional testing facility, including additional figures, are given in references 12 and 13.

Dynamic Temperature Distribution

An early goal of the investigation was to obtain a uniform dynamic temperature response over the specimen's gage length during the 200 °C temperature excursions. The temperature distribution was monitored by spot welding thirteen K-type thermocouples at 12.5 mm intervals along the central portion of the specimen as shown in figure 3. Nine of the thirteen thermocouples were located within the specimen's gage section (the central 25 mm parallel section), and the remaining four were located in the constant radius transition region. Dynamic temperature extremes in the gage length were generally within ±1 percent of the target absolute temperatures. Figure 4 shows the triangular temperature profiles measured by the six gage-section thermocouples during the first two cycles. All thermocouples were initially at the same temperature and are separated here for convenience of presentation. Thermocouples 2 and 7 were near the top extensometer probe, 3 and 8 were at the middle, and 4 and 9 were near the bottom extensometer probe. Cycle times less than 4 min resulted in excessive deviations from the

intended time-temperature profiles near the peaks and valleys because of limitations on the thermal response time of the system. In general, the linearity of the temperature waveforms improved at upper positions on the specimen (i.e., thermocouples 2 and 7) due to quicker thermal responses. As a result of this condition, temperature control was improved by locating the controlling thermocouple at an upper-gage-section location. Additional details of the method of obtaining accurate, well-controlled temperature distributions and phasing for tubular specimens are given in reference 4.

Sources of Apparent Shear Strain Measurements

In this study, apparent or artificial shear strain measurements are defined as shear strains detected or indicated by the extensometer that have no real counterpart in the specimen. Two potential sources of apparent shear strain were identified. The first is promoted by mechanical crosstalk existing in the extensometer and the second is a result of an axial misalignment of the extensometer indentations.

Many axial-torsion extensometers indicate a small apparent strain along one axis as a result of straining along the other axis. This mechanical coupling effect is commonly referred to as mechanical crosstalk. The shear strain output registered during a purely axial deformation is the component of particular interest for the present investigation. This component of apparent shear strain was a consequence of the axial strains resulting from thermal expansion during temperature cycling. The axial strains (thermal strains) during the 200 °C temperature excursions ranged from 0.004 to 0.006 m/m peak-to-peak, depending on the average coefficient of thermal expansion in a particular temperature regime. On a calibration fixture supplied by the manufacturer of the extensometer, axial strains of this magnitude resulted in apparent shear strains of about 10 μm/m. Relative to the shear strains of 0.005 m/m envisioned for a typical torsional TMD test, the mechanical crosstalk on the shear strain measurement due to axial thermal strains was deemed negligible (see additional analysis and discussion of this topic in appendix A).

Apparent shear strains due to the axial misalignment of the extensometer indentations can result from both an initial offset (due to indentation placement) and mechanical twist of the specimen. With changing temperature, the specimen will undergo expansion (or contraction) in the longitudinal, radial and circumferential directions. If the indents are not in exact alignment along the longitudinal axis (as would normally be the case during any nonzero shear strain applied during a torsion test) the circumferential change will result in a relative indent displacement and, thus, an apparent shear strain.

Investigations of the effects of indentation misalignment were carried out for cyclic temperature variations of $\pm$100 °C at various applied torques. However, given the resulting magnitudes of the apparent shear strains relative to the mechanical shear strains, this source of error was determined to be secondary. A more detailed discussion of the apparent strain effects of indentation misalignment is given in appendix A.

TORSIONAL TEST PARAMETERS AND DATA INTERPRETATION

Second Deviatoric Invariants

One common method of relating the deformation behavior of materials subjected to multiaxial loads is based on the second invariants of the deviatoric strain and stress tensors, J_2' and J_2, respectively (ref. 14):

$$J_2' = \frac{1}{6}\left[(\varepsilon_x - \varepsilon_y)^2 + (\varepsilon_x - \varepsilon_z)^2 + (\varepsilon_y - \varepsilon_z)^2\right] + \frac{1}{4}\left(\gamma_{xy}^2 + \gamma_{xz}^2 + \gamma_{yz}^2\right) \quad (3)$$

$$J_2 = \frac{1}{6}\left[(\sigma_x - \sigma_y)^2 + (\sigma_x - \sigma_z)^2 + (\sigma_y - \sigma_z)^2\right] + \tau_{xy}^2 + \tau_{xz}^2 + \tau_{yz}^2 \quad (4)$$

Use of the deviatoric component as a basis for yield (von Mises criterion) and inelastic behavior is very common, as the hydrostatic part of the stress is assumed to be unimportant for the onset of inelastic behavior of isotropic, polycrystalline metals. Assuming that the deformation behavior is similar in tension and compression (for mathematical convenience) use of the third invariant of the deviatoric stress tensor (J_3) is eliminated. Consequently, many yield and general viscoplastic constitutive theories are based exclusively on the J_2 and J_2' components of the stress and strain tensors, respectively.

One of the objectives of this study is to investigate the appropriateness of these assumptions under thermomechanical loading conditions. Through the use of existing uniaxial TMD data, parameters can be selected for the torsional TMD test which allow direct comparisons in a J_2'-J_2 stress-strain space. For example, conducting strain controlled biaxial and uniaxial tests at the same J_2' limits and J_2' rate should result in similar trends in J_2 if the material has a viscoplastic flow surface well characterized by these parameters.

Unified viscoplastic constitutive theories developed to describe a material's viscoplastic behavior often involve complex mathematical frameworks. The functional forms of such theories frequently incorporate multiple internal state variables (tensors and scalars) evolving as functions of internal state, stress, and temperature. As a result, a predicted deformation response corresponding to a specific loading condition is not straightforward or obvious. Given a viscoplastic constitutive theory where the stress is introduced through an effective value of only the J_2 component, it is obvious that by enforcing identical J_2 values for two different stress states (axial or torsional), the resulting J_2' values would be identical. However, it is not obvious that by enforcing identical J_2' values for two different strain states, the resulting J_2 values would be identical. Therefore, a representative J_2-based viscoplastic theory proposed by Robinson (refs. 15 and 16) was used to examine this condition and result. We note that in this viscoplastic formulation the flow and evolutionary laws are taken as functions of the effective (external stress minus internal stress) J_2 components. The formulation is briefly described in appendix B.

Two loading paths were used to examine the equivalence of the total J_2 paths theoretically predicted by equating the limits and rates of J_2', namely, uniaxial and torsional states. When the deformations (for any characterized material) were calculated and graphed in J_2'-J_2 space, the dual loops representing one fully-reversed load cycle fell exactly on top of one another (fig. 5). As the magnitudes of the invariants are irrelevant to the objective of the example, the invariants were normalized to their respective maximum values. Since both invariants are quadratic functions, they are always positive. Consequently, there are two J_2'-J_2 loops for every one stress-strain loop—one for the first strain-half of the cycle ($\gamma > 0$), and one for the second strain-half of the cycle ($\gamma < 0$). The results of this example demonstrate that indeed the J_2 paths predicted are equivalent for the two J_2' strain states imposed. It is reasonable to conclude that other J_2-based theories will predict identical responses in terms of J_2 when equivalent limits and rates of J_2' in uniaxial and torsional states are applied.

Based on the outcome of the above exercise, it was decided to conduct the torsional experiments at the limits of J_2' dictated by the existing uniaxial TMD database for Hastelloy X (ref. 1). Here the goal was to determine whether or not the resulting deformations in the two types of tests could be correlated

in a J_2'-J_2 space. The uniaxial TMD tests were conducted with fully reversed constant mechanical strain amplitudes. The expression for J_2' under a uniaxial state of stress is given by

$$J_2' = \frac{\varepsilon^2}{3}(1 + \nu^{\text{eff}})^2 \tag{5}$$

where ε is the corresponding axial strain component and ν^{eff} is the effective Poisson's ratio. Full strain tensor measurements for uniaxial TMD tests were not available; therefore, the rule of mixtures expression for ν^{eff} was used to estimate the missing transverse strains required to calculate J_2':

$$\nu^{\text{eff}} = \frac{\nu^{\text{el}}\varepsilon^{\text{el}} + \nu^{\text{pl}}\varepsilon^{\text{pl}}}{\varepsilon^{\text{el}} + \varepsilon^{\text{pl}}} \tag{6}$$

In equation (6), superscripts "el" and "pl" refer to elastic and plastic components, respectively. The temperature dependent values used for ν^{el} were taken from reference 17. These values were generated from the same heat of material used for the torsional specimens in this study. The assumed value for ν^{pl} was 0.5. In calculating the J_2' values for any given uniaxial TMD cycle, two values for ν^{eff} were used: one for $\varepsilon > 0$ and a second for $\varepsilon < 0$. These two values of ν^{eff} were calculated based on the temperatures and $\varepsilon^{\text{el}}/\varepsilon^{\text{pl}}$ ratios existing at the maximum and minimum strain limits of the cycle, respectively. This method closely approximated a point-by-point calculation of ν^{eff}. Note that as the material experiences a change in the $\varepsilon^{\text{el}}/\varepsilon^{\text{pl}}$ ratio (i.e., the uniaxial cyclic stress increases or decreases) under fully reversed constant mechanical strains, ν^{eff} will change and, hence, the J_2' limits for each cycle will change during a constant uniaxial strain test.

The value of J_2' in a torsion test is given by the expression:

$$J_2' = \frac{\gamma^2}{4} \tag{7}$$

Clearly, there is no dependence on any unmeasured strains in the above expression. Hence, there is a simple, proportional relationship between J_2' and the applied shear strain, γ. Furthermore, unlike the uniaxial case, a constant shear strain amplitude test implies a constant J_2' amplitude test.

It was not desirable (or trivial) to conduct the torsional TMD experiments with variable J_2' limits to mimic the uniaxial J_2' limits throughout the course of the test. Therefore, the torsional TMD J_2' limits were chosen to match those found in the first cycle of the uniaxial TMD data. Because the J_2' limits are matched only during the first deformation cycle, the forthcoming comparisons of J_2 and J_2' in torsional and uniaxial TMD tests are restricted to include only the first cycle.

A question remains concerning the equivalence of J_2' rates in the uniaxial and torsional tests due to the variation in the Poisson's ratio in the uniaxial tests over the course of the cycle. That is, does the triangular axial mechanical strain waveform used in the uniaxial test correspond to a triangular shear strain waveform in the torsion test if we are trying to maintain identical J_2' values throughout the cycle? The question can be addressed by taking uniaxial stress-strain data for a given cycle and computing the corresponding equivalent shear strains on a point-by-point basis. The result of such a calculation is shown in figure 6. Superposed on the discrete values of equivalent shear strain is a triangular waveform representing the actual control variable during a torsional test. It is clear that the equivalent shear

strains fall quite closely to the triangular waveform. This indicates that the triangular shear strain waveform will closely approximate the variation of J_2' resulting from the triangular uniaxial strain waveform.

In summary, it has been shown that if we can measure or calculate limits of J_2' for a particular cycle from a strain amplitude-controlled uniaxial TMD test, we can easily duplicate these values of J_2' in a strain-controlled torsion test, such that the applied J_2' waveforms, rates, and limits are nearly identical for that cycle in both tests.

TEST MATRIX

The test matrix showing the limits and sequences of temperature and strain for torsional and uniaxial specimens is given in table II. Because the shear strain limits of the torsional experiments were chosen to match the J_2' limits experienced on the first cycle of the strain-controlled uniaxial TMD tests, the shear strain limits in table II are not necessarily fully-reversed. The uniaxial mechanical strain limits were fully reversed.

The temperature ranges for the torsional test matrix were selected based on previous experience with uniaxial TMD of Hastelloy X (ref. 1) which revealed that the 400 to 600 °C temperature regime results in increased hardening because it maximizes the combined strain aging effects of carbide precipitation and solute drag. The 600 to 800 °C temperature range also provokes significant hardening at 600 °C, but strong thermal recovery mechanisms at 800 °C lessen the hardening at the cold extreme of the cycle (relative to that at either extreme of the 400 to 600 °C temperature regime) and induce softening at the hot extreme of the cycle. Hastelloy X saturated immediately in the 800 to 1000 °C temperature regime in the previous uniaxial experiments, and therefore exhibited no softening or hardening.

RESULTS AND DISCUSSION

Initial cyclic stress-strain loops (up to the third strain reversal) for the in-phase and out-of-phase torsional tests are shown in figure 7. By the third strain reversal, the 400 to 600 °C loop is nearly symmetric about zero stress, while the deformation responses at higher temperatures exhibit notable mean stresses. Note the significant loss of load-carrying capability (stress relaxation) of the 800 to 1000 °C TMD specimens, particularly at the 1000 °C limit. Also evident is the decreasing slope of the unloading path with increased temperatures. Technically, one cannot infer a shear modulus from such slopes due to the time-dependent deformation and changing temperature during the loading cycle. However, for a fixed thermomechanical loading regime, cycle-dependent changes in the slope of the unloading path would qualitatively indicate a metallurgical change and/or damage development in the material being tested. This occurrence will be pointed out subsequently.

Substantial cyclic stress hardening is evident in the stress-strain loops shown in figure 8 for the 400 to 600 °C IP and OP tests, particularly at the 400 °C temperature limit as evidenced best by the longer duration in-phase test. Specimens tested in the 600 to 800 °C range revealed substantial hardening at the 600 °C limit and softening at the 800 °C limit (fig. 9). An interesting feature in the IP and OP 600 to 800 °C tests that was not observed in the uniaxial tests is the decreasing slope of the unloading path from the 800 °C limit with respect to cycles. The slope of the unloading path in the cooler half of the cycle remained essentially constant, however. An additional 600 to 800 °C test not included in this paper displayed similar behavior, supporting the repeatability of this result. A detailed microstructural investigation would be needed in order to determine whether or not physical changes in the alloy

promoted this phenomenon. No sequential stress-strain loops for the 800 to 1000 °C tests are included herein because the material was essentially cyclically neutral throughout both the IP and OP tests.

As evidence of the repeatability of the hardening trends, duplicate 400 to 600 °C IP tests are shown in figure 10 (ATHX1 was prematurely terminated due to a heater malfunction and therefore excluded from the test matrix). The shear stress values have been normalized with respect to their first cycle values. Normalized shear stresses in this comparison were measured at the point of shear strain reversal. The agreement between the two data sets is exceptionally good. Also clearly evident by the hardening trends is the initially higher rate of hardening at the 600 °C temperature limit up to about 100 cycles, followed by an accelerated hardening rate (on a log scale) at the 400 °C temperature limit beginning at about 500 cycles. This behavior is similar to that observed during the uniaxial TMD testing of Hastelloy X in this temperature range where a greater degree of hardening was found to result from the combined effects of solute drag and precipitation hardening (refs. 1 and 11).

An interesting axial-torsional interactive effect observed in the torsional tests is axial strain ratchetting. This phenomenon is often referred to as the Poynting-Swift effect (refs. 18 to 20). The maximum and minimum axial strains of select cycles are shown in figure 11 for two extreme examples. The first example is a 800 to 1000 °C IP test in which 0.0018 m/m axial strain accumulated within 40 cycles; the second is a 600 to 800 °C IP test in which −0.0018 m/m axial strain accumulated after 2700 cycles. In all tests but one, axial strain ratchetted in the positive direction. A comprehensive investigation of the room-temperature axial ratchetting phenomenon by Wack (ref. 21) with several metallic materials in torsion led to the following conclusions: the sign of the axial ratchet is theoretically positive; the amount of ratchet per cycle seems material dependent, is highly influenced by axial forces, and is sensitive to the loading history. Since the present experiments were conducted at elevated temperatures at which viscous effects are significant, the relative influence of the factors cited by Wack may differ. For example, the average rates of axial ratchetting in the 800 to 1000 °C tests were up to 2 orders of magnitude greater than those seen in the lower temperature regimes. As the ratchetting required at least several cycles (in the extreme case) before it accumulated to a measurable quantity, it was felt to have no influence on the first-cycle deformation and corresponding values of J_2'.

Comparisons of first-cycle thermomechanical deformations in the J_2'-J_2 space are given for the three temperature ranges in figures 12 to 15. In these figures, coincidental zero values of both J_2' and J_2 exist only at the start of the test. Overall, the correlations of the uniaxial and torsional data were excellent in the 800 to 1000 °C temperature range (fig. 12). The only portion of this loop where the data did not agree exceptionally well is the initial loading. This may be a result of the slight error introduced in the uniaxial J_2' calculations based on the assumptions of using ν^{eff}. The 600 to 800 °C data also resulted in fairly good agreement (fig. 13). This result clearly suggests that the multiaxial TMD behavior of Hastelloy X is well characterized by the scalar parameter J_2 at these temperatures.

In contrast to the higher-temperature correlations, the 400 to 600 °C IP and OP correlations (figs. 14 and 15, respectively) were not good, particularly during the second strain-half of the cycle. Note that the Bauschinger effect was much more pronounced in the IP and OP uniaxial loading cases. Unfortunately, because of the thermomechanical nature of the cycle (i.e., the continually changing elastic modulus) it is difficult to isolate or quantify this effect.

Recall that the 400 to 600 °C temperature range is where the most hardening occurs due to the interaction of carbide precipitation and solute drag (refs. 1 and 11). Considering that the hardening is greatest in this temperature range, the results suggest that the hardening mechanisms active in torsional TMD are significantly different from those in uniaxial TMD. Deformation behaviors may be slightly influenced by the heat of material from which the specimens were fabricated, but this is not a likely explanation for

the significant differences seen here. In the 400 to 600 °C temperature range, a J_2-based description of the viscoplastic deformation does not appear capable of collapsing the axial and torsional TMD. In similar fashion, other investigators have also seen increased isothermal hardening (with a cobalt-base superalloy) in torsional deformation versus axial deformation when the tests are compared with Von Mises-type stresses and strains (ref. 22).

CONCLUSIONS

Techniques developed under uniaxial conditions to control mechanical strain/temperature phasing were effectively transferred to torsional TMD conditions. The TMD tests were conducted in strain control without compensation for thermal strains. This is the primary advantage of torsional, strain-controlled TMD testing over uniaxial, strain-controlled TMD testing where thermal strain compensation introduces control complexities. However, with the extensometry employed in this study, secondary sources of error may arise under TMD conditions relating to apparent shear strain measurements promoted by indent misalignment and extensional strain ratchetting. A simple analysis revealed that the magnitudes of these errors are negligible.

Based on the limited amount of data generated, the following conclusions can be made concerning the hardening of Hastelloy X during TMD in torsion: (a) the 400 to 600 °C tests resulted in the most hardening, particularly at the 400 °C temperature limit; (b) the 600 to 800 °C tests resulted in hardening at the 600 °C temperature limit and softening at the 800 °C limit; and (c) the 800 to 1000 °C tests resulted in a saturated material response at both temperature limits. All temperature ranges investigated resulted in nonzero mean shear stresses.

First-cycle thermomechanical torsional and uniaxial deformations were compared. The experiments were based on forcing identical values for the second invariant of deviatoric strain tensor (J_2') and comparing the resulting values for the second invariant of the deviatoric stress tensor (J_2). The following results were obtained: (a) excellent correlation was exhibited in the 800 to 1000 °C TMD tests; (b) fairly good correlation was obtained in the 600 to 800 °C TMD tests; and (c) fair to poor correlations were experienced in the 400 to 600 °C TMD tests. The results suggest that the deformation of Hastelloy X is well described by a classical J_2-based viscoplastic theory in the upper temperature ranges where reduced kinematic hardening takes place and recovery effects are dominant. In those temperature ranges involving substantial kinematic hardening (e.g., 400 to 600 °C), the hardening mechanisms active in uniaxial and torsional loadings appear significantly different: the Bauschinger effect in the 400 to 600 °C uniaxial TMD was consistently stronger. In those cases, the deformation loops did not agree in the J_2'-J_2 state space.

ACKNOWLEDGMENTS

The second author would like to thank the NASA/ASEE fellowship program for providing the funding that made possible his summer residence at NASA Lewis Research Center, where this work was carried out. The authors also wish to acknowledge S. Arnold, P. Bonacuse, A. Freed, and S. Kalluri for their insightful discussions on the experimental and analytical aspects of this work. Also, technical assistance in the laboratory from C. Burke, R. Corner, D. Pech, R. Shinn, and S. Smith, is greatly appreciated.

APPENDIX A—BASIC CONSIDERATIONS ON SHEAR STRAIN MEASUREMENT WITH DUAL PROBE EXTENSOMETERS

Preamble

The problem at hand is to measure engineering shear strain in a thin-walled tubular specimen with a dual probe extensometer during a pure-torsion thermomechanical deformation test. The geometric relationships between total shear strain, γ, the total length between the probes, l, and the total lateral displacement of the lower probe, s (hereafter referred to as the sector), are shown in fig. A1(a). Figure A1(b) shows the angle of twist, ϕ, in relation to the sector, s, and the mean radius of the specimen, r. In this discussion, sources of error in shear strain measurement due to temperature change, extensional strain ratchetting, and dimple misalignment are addressed. It is assumed that the thermomechanical properties of the material are isotropic.

Development of Basic Equations

The total engineering shear strain, γ, is related to the angle of twist by the expression

$$\gamma = \frac{r\phi}{l} \tag{A1}$$

The total axial gage length measured by a dual-probe extensometer can be expressed as

$$l = l_0 + \Delta l_T + \Delta l_R \tag{A2}$$

where l_0 is the initial axial gage length (before thermal and ratchetting effects) and Δl_T and Δl_R are the changes in length due to thermal and ratchetting strains, respectively. Hereafter, a nominal value of 25 mm will be assumed for l_0. The two length changes can be expressed in terms of their respective strain components as follows:

$$\Delta l_T = \alpha \Delta T l_0 \tag{A3}$$

$$\Delta l_R = \epsilon_{LR} l_0 \tag{A4}$$

where $\alpha\Delta T$ is the longitudinal thermal strain and ϵ_{LR} is the longitudinal ratchetting strain (observed and noted in the present and previous investigations (refs. 18 to 21)). Hence, the total length becomes

$$l = l_0(1 + \alpha \Delta T + \epsilon_{LR}) \tag{A5}$$

The total values of twist angle, shear strain, and sector can be separated into components associated with mechanical loading (subscript m) and initial dimple misalignment (subscript i).

$$\phi = \phi_m + \phi_i \tag{A6}$$

$$\gamma = \gamma_m + \gamma_i \tag{A7}$$

$$s = s_m + s_i \tag{A8}$$

Of the terms in the previous three equations, s_m, s_i, γ_m, and γ_i are influenced by thermal and ratchetting strains in ways which will be described later. For example, γ_m includes both mechanical shear strain and additional (nonmechanical) shear strain due to thermal and ratchetting effects that arise due to the presence of mechanical shear strain.

Using equation (A8) and the simple relationship between mechanical twist and mechanical sector,

$$s_m = r\phi_m \tag{A9}$$

we have

$$s = r\phi_m + s_i \tag{A10}$$

where the radius, r, can be expressed in terms of its original value measured after specimen fabrication, r_0, and changes due to thermal and ratchetting effects, Δr_T and Δr_R, respectively.

$$r = r_0 + \Delta r_T + \Delta r_R \tag{A11}$$

In terms of the thermal and ratchetting strains in the hoop direction ($\alpha\Delta T$ and ε_{HR}, respectively), the expression for r becomes

$$r = r_0(1 + \alpha\ \Delta T + \varepsilon_{HR}) \tag{A12}$$

The initial lateral dimple misalignment is affected by thermal and ratchetting strains in a similar fashion.

$$s_i = s_{i0}(1 + \alpha\ \Delta T + \varepsilon_{HR}) \tag{A13}$$

Here, s_{i0} is the original dimple misalignment due to less than ideal specimen preparation. Combining equations (A10) to (A13), we have

$$s = (r_0\phi_m + s_{i0})(1 + \alpha\ \Delta T + \varepsilon_{HR}) \tag{A14}$$

from which we conclude that

$$s_m = \tilde{s}_m(1 + \alpha\ \Delta T + \varepsilon_{HR}) \tag{A15}$$

where the actual (excluding thermal and ratchetting effects) mechanically-induced sector, $\tilde{s}_m$, defined as

$$\tilde{s}_m = \phi_m r_0 \tag{A16}$$

is the quantity we desire to control in a torsional TMD test due to its unchanging value with thermal and ratchetting strains. Substitution of equations (A5) and (A14) into equation (A1) provides the final expression for shear strain in terms of all the stated effects.

$$\gamma = \frac{s}{l} = \frac{(\tilde{s}_m + s_{i0})(1 + \alpha\ \Delta T + \varepsilon_{HR})}{l_0(1 + \alpha\ \Delta T + \varepsilon_{LR})} \tag{A17}$$

Expressing equation (A17) in the form of equation (A7), we have

$$\gamma_m = \frac{\tilde{s}_m(1 + \alpha\ \Delta T + \varepsilon_{HR})}{l_0(1 + \alpha\ \Delta T + \varepsilon_{LR})} \tag{A18}$$

and

$$\gamma_i = \frac{s_{i0}(1 + \alpha\ \Delta T + \varepsilon_{HR})}{l_0(1 + \alpha\ \Delta T + \varepsilon_{LR})} \tag{A19}$$

Determination of Initial Dimple Misalignment and Extensometer Cross-Talk

The original dimple misalignment, s_{i0}, may be directly measured by inspecting the dimpled specimen with an optical comparator or traveling stage microscope. Alternatively, s_{i0} may be found by imposing thermal cycles onto the instrumented specimen while maintaining zero torque. In the latter method, an additional source of inaccuracy—namely, mechanical cross-talk between the axial and torsional outputs of the extensometer—can be accounted for in a very convenient manner. The procedure is as follows:

(a) Mount the specimen in the load frame in load control and zero both extensometer channels.

(b) Impose the mean test temperature on the specimen and measure the change in the twist angle, ϕ (just ϕ_i, here). An apparent shear strain due to initial dimple misalignment, γ_i, can then be calculated by substituting equations (A5), (A6), and (A11) into equation (A1), with the final result being:

$$\gamma_i = \frac{\phi_i r_0}{l_0} \tag{A20}$$

(c) Using equation (A17), the total shear strain induced by this temperature change is theoretically given by

$$\gamma_i = \frac{s_{i0}}{l_0} \tag{A21}$$

which, importantly, is independent of ΔT and α. This fact eliminates concern about temperature-dependent thermal expansion coefficients. The original dimple misalignment, s_{i0}, can now be calculated by equating equations (A20) and (A21), with the result being:

$$s_{i0} = \phi_i r_0 \tag{A22}$$

A typical value of s_{i0} found in this manner was about ± 5 μm. The original dimple misalignment will influence measured sectors when thermal and ratchetting strains exist.

Before switching to strain control and beginning the test (the specimen is presently at the mean test temperature, T_m), the torsional strain channel must be re-zeroed, as it will now reflect the strain resulting from the dimple misalignment. Mathematically, the value being zeroed can be expressed as

$$s^* = s_{i0}\left[1 + \alpha(T_m - T_{RT})\right] \tag{A23}$$

making the expression for the actual shear strain (A17), measured relative to the mean test temperature,

$$\gamma = \frac{(s_{m0} + s_{i0})(1 + \alpha\ \Delta T + \varepsilon_{HR}) - s^*}{l_0(1 + \alpha\ \Delta T + \varepsilon_{LR})} \tag{A24}$$

Note that the value of s_{i0} found via equation (A22) will also include any existing axial-torsional cross-talk component (inherent in most dual-probe extensometers). That is, the effects of original dimple misalignment and extensometer cross-talk are indistinguishable during temperature changes (with no mechanical loading). However, the cross-talk component can be easily determined prior to the test. This is accomplished on the extensometer's calibration stand by imposing strains (i.e., displacements) on one axis and monitoring the cross-talk strains on the other. Having established the cross-talk strain values, appropriate adjustments to the value of s_{i0} can be made if necessary.

Significance of Various Sources of Error in Shear Strain Measurements with Dual Probe Extensometers

As an example, suppose that the shear strain desired in a torsional TMD test, γ', is 0.005 m/m. The resulting sector imposed on the specimen by the load frame operated in strain control is found by the following expression:

$$s = \gamma' l_0 \tag{A25}$$

where $l_0 = 25$ mm in the present case. The actual value of shear strain thereby imposed on the specimen as it undergoes temperature changes and ratchetting strains is found by dividing the actual sector by the actual length between the probes.

$$\gamma = \frac{\gamma' l_0}{l_0(1 + \alpha\ \Delta T + \varepsilon_{LR})} \tag{A26}$$

The percent difference between the shear strain achieved and that desired is defined as

$$\text{err} = \left(\frac{\gamma}{\gamma'} - 1 \right) \times 100\% \tag{A27}$$

which upon rearrangement of equation (A26) is

$$\text{err} = \left[\frac{1}{(1 + \alpha\ \Delta T + \varepsilon_{LR})} - 1 \right] \times 100\% \tag{A28}$$

Given representative values of α, ΔT, and ε_{LR} for the present investigation

$$\alpha = 17 \text{ x } 10^{-6}\ /^{\circ}C$$

$$\Delta T = \pm 100\ ^{\circ}C$$

$$\varepsilon_{LR} = \pm 2000\ \mu\varepsilon$$

the error is ± 0.37 percent—a value which is hardly consequential in practice.

Conclusion

Some basic expressions for the various factors affecting shear strain measurements in torsion TMD tests have been presented and assessed for their importance in the present investigation. It has been shown that the effects of dimple misalignment, thermal excursions, and extensional strain ratchetting are secondary and can therefore be neglected. The results of this simple analysis and the clean deformation loops measured in the laboratory all support the validity of the torsional TMD control algorithm developed in this investigation.

APPENDIX B—MATHEMATICAL FRAMEWORK OF A UNIFIED VISCOPLASTIC THEORY PROPOSED BY ROBINSON

The general mathematical framework used in the Robinson model evolves from a class of constitutive equations originally derived from the gradient of a complementary dissipation potential function, Ω. This function is defined as follows.

$$\Omega = \Omega(\sigma_{ij}, \alpha_{ij}, T) \tag{B1}$$

$$\Omega = \Omega(F,G,T) = \theta_f(T) \int f(F)dF + \theta_g(T) \int g(G)dG \tag{B2}$$

where

$$F = \frac{\tilde{J}_2}{K^2} - 1 \quad \text{and} \quad G = \frac{\hat{J}_2}{K^2}$$

$$\tilde{J}_2 = \frac{1}{2}\Sigma_{ij}\Sigma_{ij} \qquad \Sigma_{ij} = S_{ij} - a_{ij}$$

$$\hat{J}_2 = \frac{1}{2}a_{ij}a_{ij} \qquad a_{ij} = \alpha_{ij} - \frac{1}{3}\alpha_{kk}\delta_{ij}$$

$$S_{ij} = \sigma_{ij} - \frac{1}{3}\sigma_{kk}\delta_{ij}$$

Here σ_{ij} is the *applied* stress, α_{ij} is the *internal* (or *back*) stress, and T is the temperature. For initially isotropic materials, Ω can be taken (refs. 15 and 16) to depend upon the second invariants of deviatoric stress quantities through scalar functions **F** and **G**. The applied stress dependence enters through **F** which plays the role of a Bingham-Prager yield function; the *drag* stress K is taken to be constant and plays the role of a Bingham threshold shear stress (ref. 23), below which the inelastic stain rate vanishes. Models developed from this potential/normality structure have been shown (ref. 24) to be consistent with a simple thermodynamic formalism. Also, this general framework has been used (refs. 15, 16, 25, and 26) as a starting point for various viscoplastic models of isotropic and anisotropic metals.

Shown below are the flow law $\left(\dot{\varepsilon}_{ij}^{in}\right)$ for the inelastic strain, and the evolutionary law for the deviatoric *internal* stress ($\mathbf{a}_{ij}$), obtained by differentiating the dissipation potential function (Ω) with respect to the *applied* stress, and *internal* stress, respectively.

$$\dot{\varepsilon}_{ij}^{in} = \frac{\partial\Omega}{\partial\sigma_{ij}} = \frac{\theta_f(T)}{K^2} f(F)\Sigma_{ij} \tag{B3}$$

$$\dot{a}_{ij} = -h(\alpha_{kl},T)\frac{\partial\Omega}{\partial\alpha_{ij}} = h(G)\dot{\varepsilon}_{ij} - \theta_g(T)\rho(G)a_{ij} \tag{B4}$$

where

$$\rho(G) = h(G)g(G)$$

The functions θ_f and θ_g are typically taken with Arrhenius forms.

The assumed dependence of functions $\mathbf{F}$ and $\mathbf{G}$ on the second deviatoric invariants of the effective and *internal* stresses implies full isotropy of the material (ref. 27). Note that in typical fashion there is no dependence on the third invariant of the deviatoric stress tensor, J_3. Thus, the second deviatoric invariants of *applied* stress and *internal* stress (J_2-type quantities) clearly control the evolution of the inelastic strain and *internal* stress.

REFERENCES

1. Castelli, M.G.; Miner, R.V.; and Robinson, D.N.: Thermomechanical Deformation Behavior of a Dynamic Strain Aging Alloy, Hastelloy X. To be published in Thermo-Mechanical Fatigue Behavior of Materials, STP–1186, H. Sehitoglu, ed., American Society for Testing and Materials, Philadelphia, PA, 1993.

2. Murakami, S.; Kawai, M.; and Ohmi, Y.: Effects of Amplitude-History and Temperature-History on Multiaxial Cyclic Behavior of Type 316 Stainless Steel. J. Eng. Mater. Technol., vol. 111, no. 3, July 1989, pp. 278–285.

3. Bhattachar, V.; and Stouffer, D.C.: A Constitutive Model for the Thermomechanical Fatigue Response of René 80. Presented at the Sixth TMF Workshop, NASA Lewis Research Center, Cleveland, OH, June 5-6, 1991.

4. Castelli, M.G.; and Ellis, J.R.: Improved Techniques for Thermomechanical Testing in Support of Deformation Modeling. To be published in Thermo-Mechanical Fatigue Behavior of Materials, STP–1186, H. Sehitoglu, ed., American Society for Testing and Materials, Philadelphia, PA, 1993.

5. Hopkins, S.W.: Low-Cycle Thermal Mechanical Fatigue Testing. Thermal Fatigue of Materials and Components, STP–612, D.A. Spera and D.F. Mowbray, eds., American Society for Testing and Materials, Philadelphia, PA, 1976, pp. 157–169.

6. Jones, W.B.; Schmale, D.T.; and Bourcier, R.J.: A Test System for Computer-Controlled Thermomechanical Fatigue Testing. Report SAND–88–2183C, Sandia National Labs., Albuquerque, NM, 1988.

7. Ellis, J.R.; and Robinson, R.N.: Some Advances in Experimentation Supporting Development of Viscoplastic Constitutive Models. NASA CR–174855, 1985.

8. Jordan, E.H.: Biaxial Thermo-Mechanical Fatigue. 4th Annual Hostile Environments and High Temperature Measurements Conference, Proceedings, Society for Experimental Mechanics, Bethel CT, 1987, pp. 1–6.

9. Bonacuse, P.J.; and Kalluri, S.: Axial-Torsional Fatigue: A Study of Tubular Specimen Thickness Effects. NASA TM–103637, 1990.

10. Ellis, J.R.; and Bartolotta, P.A.: Adjustable Induction Heating Coil. NASA Tech. Brief, vol. 14, no. 11, Nov. 1990, p. 50.

11. Miner, R.V.; and Castelli, M.G.; Hardening Mechanisms in a Dynamic Strain Aging Alloy, Hastelloy X, During Isothermal and Thermomechanical Cyclic Deformation. Metall. Trans., vol. 23A, Feb. 1992, pp. 551–562.

12. Bartolotta, P.A.; and McGaw, M.A.: A High Temperature Fatigue and Structures Testing Facility. NASA TM–100151, 1987.

13. Bonacuse, P.J.; and Kalluri, S.: Results of Inphase Axial-Torsional Fatigue Experiments on 304 Stainless Steel. NASA TM–101464, 1989.

14. Mendelson, A.: Plasticity: Theory and Application, Krieger, Malabar, FL, 1983.

15. Robinson, D.N.: A Unified Creep-Plasticity Model for Structural Metals at High Temperature. Report ORNL/TM–5969, Engineering Technology Div., Oak Ridge National Labs., Oak Ridge, TN, Oct. 1978.

16. Robinson, D.N.; and Swindeman, R.W.: Unified Creep-Plasticity Constitutive Equations for Structural Alloys at Elevated Temperatures. Report ORNL/TM–8444, Engineering Technology Div., Oak Ridge National Labs., Oak Ridge, TN, Oct. 1982.

17. Kalluri, S.; and Bonacuse, P.J.: A Data Acquisition and Control Program for Axial-Torsional Fatigue Testing. Applications of Automation Technology to Fatigue and Fracture Testing, STP–1092, A.A. Braun, N.E. Ashbaugh, and F.M. Smith, eds., American Society for Testing and Materials, Philadelphia, PA, 1990, pp. 269-287.

18. Poynting, J.H.: Pressure Perpendicular to Shear Planes and Lengthening of Wires When Tested. R. Soc. London Proc., Ser. A, vol. 82, July 1909, pp. 546–559.

19. Poynting, J.H.: Changes in Dimensions of a Steel Wire When Tested and Pressure of Distortional Waves in Steel. R. Soc. London Proc., Ser. A, vol. 86, June 1912, pp. 543–561.

20. Swift, H.W.: Length Changes in Metals Under Torsional Overstrain. Engineering, vol. 163, 1947, pp. 253–257.

21. Wack, B.: The Torsion of a Tube (or a Rod): General Cylindrical Kinematics and some Axial Deformation and Ratchet Measurements. Acta Mech., vol. 80, 1989, pp. 39–59.

22. Bonacuse, P.J.; and Kalluri, S.: Elevated Temperature Axial and Torsional Fatigue Behavior of Haynes 188. NASA TM–105396, 1992.

23. Bingham, E.C.: Fluidity and Plasticity, McGraw-Hill, NY, 1922.

24. Ponter, A.R.S.: General Theorems for the Dynamic Loading of Structures for a State Variable Description of Material Behavior. Mechanical Properties at High Rates of Strain, 1979; Proceedings of the Second Conference, J. Harding, ed., (Institute of Physics Conference Series, No. 47), Bristol, England, 1980, pp. 130–141.

25. Robinson, D.N.: Constitutive Relationships for Anisotropic High Temperature Alloys. Nucl. Eng. Design, vol. 83, 1983, pp. 389-396.

26. Robinson, D.N.; Duffy, S.F.; and Ellis, J.R.: A Viscoplastic Constitutive Theory for Metal Matrix Composites at High Temperatures. Thermal Stress, Material Deformation, and Thermo-Mechanical Fatigue; Proceedings of the 1987 Pressure Vessels and Piping Conference, ASME, New York, 1987, pp. 49–56.

27. Sadegh, A.M.; and Cowin, S.C.: The Proportional Anisotropic Elastic Invariants. J. Appl. Mech., vol. 58 1991, pp. 50–57.

TABLE I.—CHEMICAL COMPOSITION OF THE MATERIAL HEATS OF HASTELLOY X

Element	Torsion heat	Uniaxial heat
	Composition, wt.%	
C	0.084	0.069
Mn	.55	.58
Si	.64	.48
S	.001	.001
P	.021	.022
Cr	20.83	21.11
W	.37	.40
Ni	Balance	Balance
Mo	8.74	8.46
Co	1.65	1.72
Cu	---------	.09
Al	---------	.06
Ti	---------	<.02
Fe	18.42	18.88
B	.0036	.0040

TABLE II.—TEST MATRIX

Torsional specimen	Temperature[a]/ strain sequeuce	Temperature range, °C	Engr. shear strain limits maximum/minimum, m/m	Corresponding uniaxial specimen[b]
ATHX10	H, C/+,−	400 to 600	0.00520/−0.00517	UHX458
ATHX11	C, H/+,−	400 to 600	.00516/−.00520	UHX448
ATHX6	H, C/+,−	600 to 800	.00537/−.00538	UHX467
ATHX15	C, H/+,−	600 to 800	.00519/−.00512	UHX484
ATHX9	H, C/+,−	800 to 1000	.00534/−.00523	UHX459
ATHX12	C, H/+,−	800 to 1000	.00517/−.00530	UHX491

[a]H and C correspond to Hot and Cold temperature limits.
[b]All uniaxial specimens were cyclically loaded at ±0.0030 m/m mechanical strain.

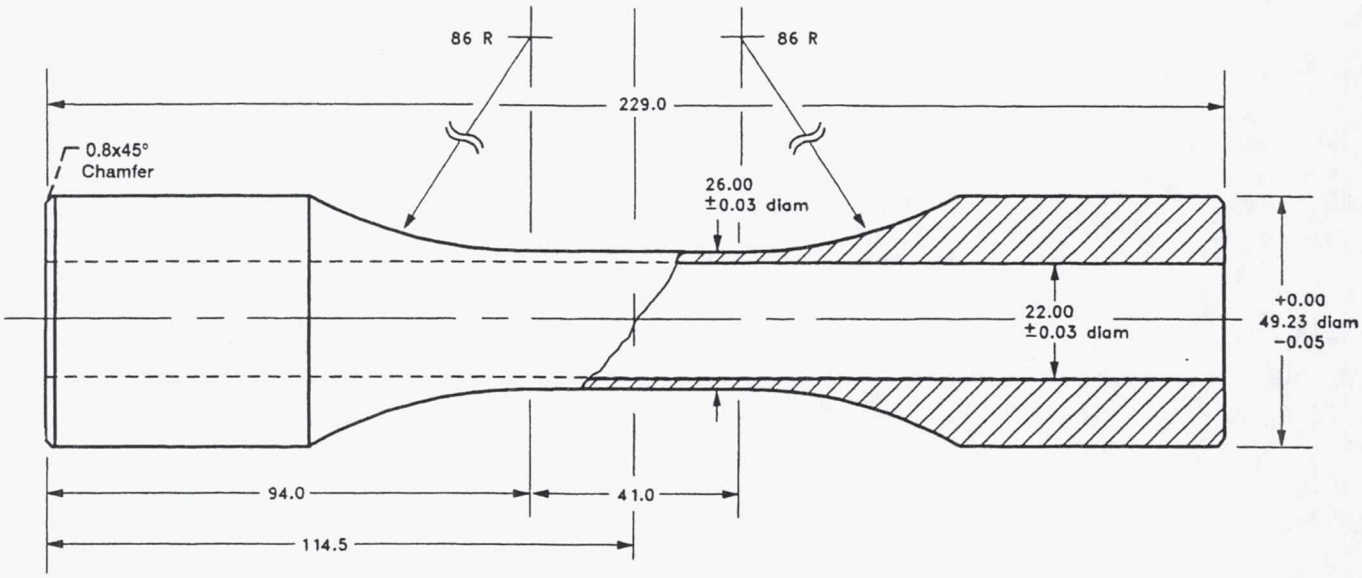

(a) Torsion.

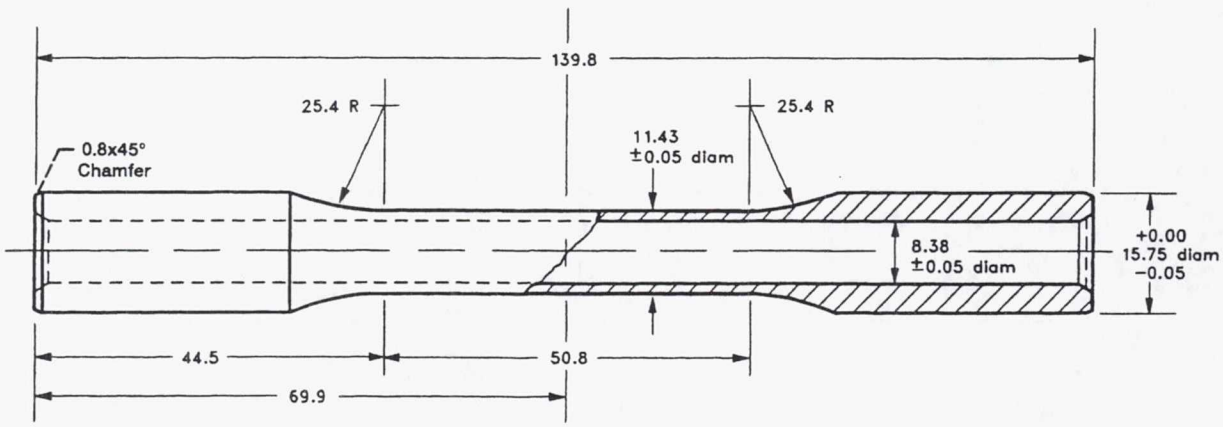

(b) Uniaxial.

Figure 1.—Test specimen geometries.

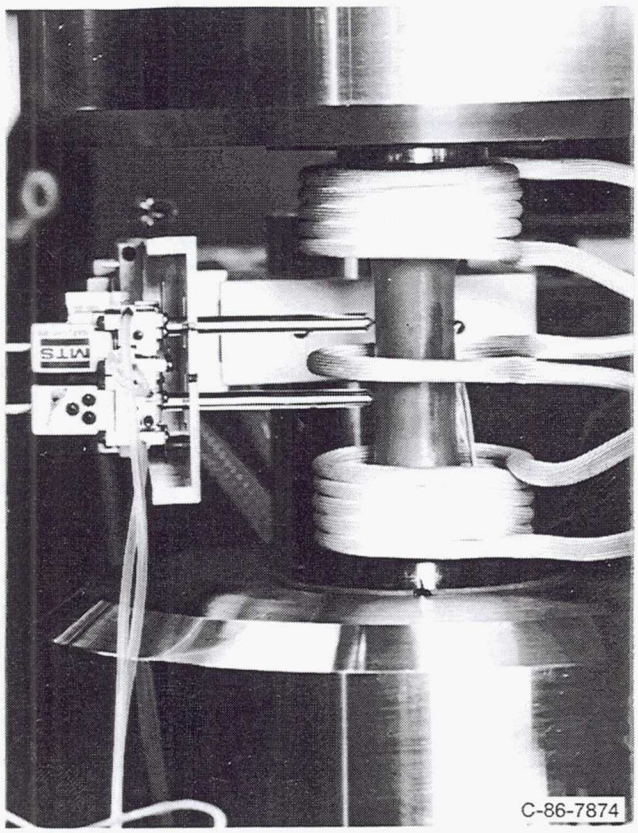

Figure 2.—Torsional test apparatus showing instrumented specimen in place.

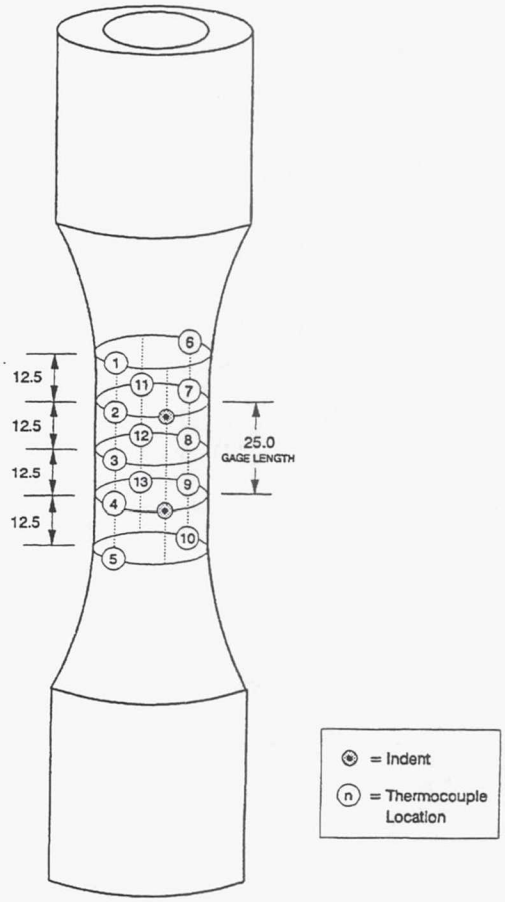

Figure 3.—Extensometer indents and thermocouple locations on a torsional test specimen. (Dimensions are in millimeters.)

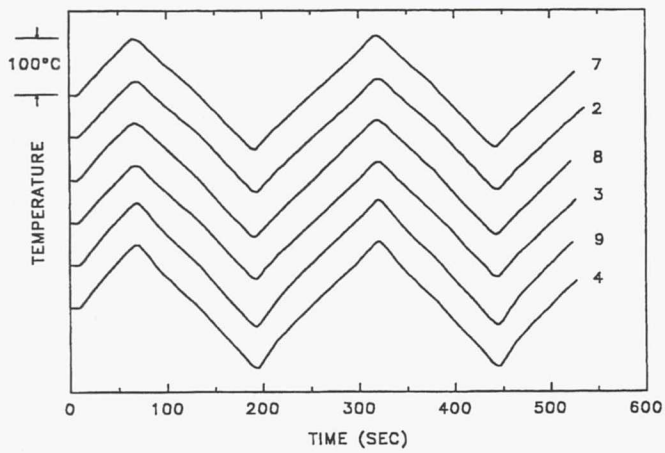

Figure 4.—Triangular temperature waveforms measured by gage-section thermocouples during the first two thermal cycles.

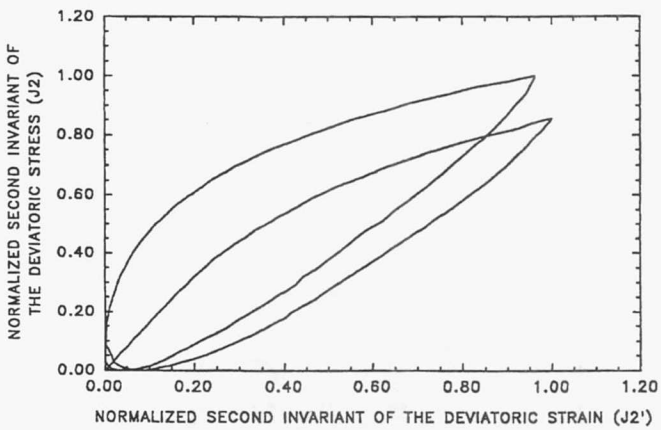

Figure 5.—Predicted viscoplastic deformation in J_2'-J_2 space of a hypothetical material which obeys J_2-based constitutive laws during either shear or uniaxial loading at common limits and rate of J_2'.

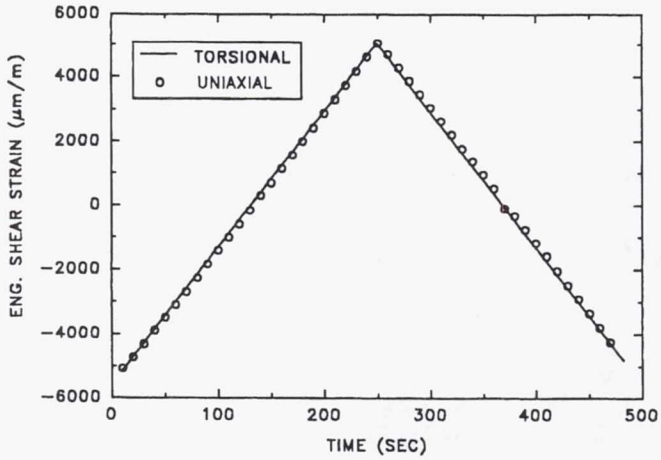

Figure 6.—Variation of equivalent shear strain from a uniaxial test and actual shear strain from a torsional test.

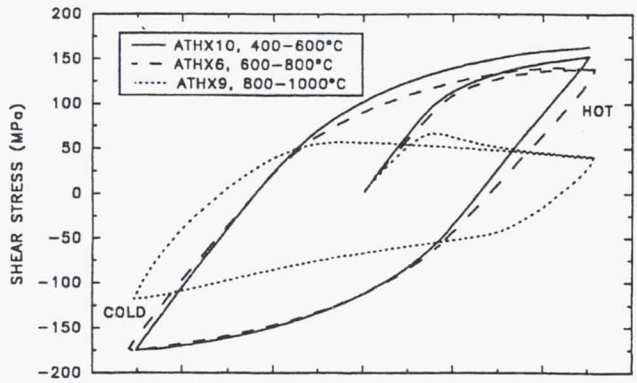

(a) In-phase.

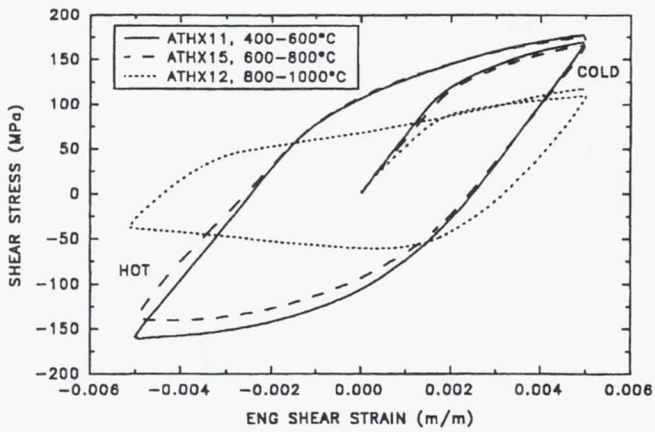

(b) Out-of-phase.

Figure 7.—Initial stress-strain loops for torsional tests.

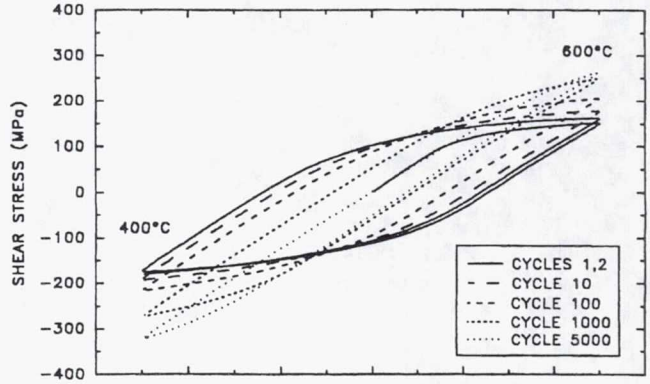

(a) In-phase.

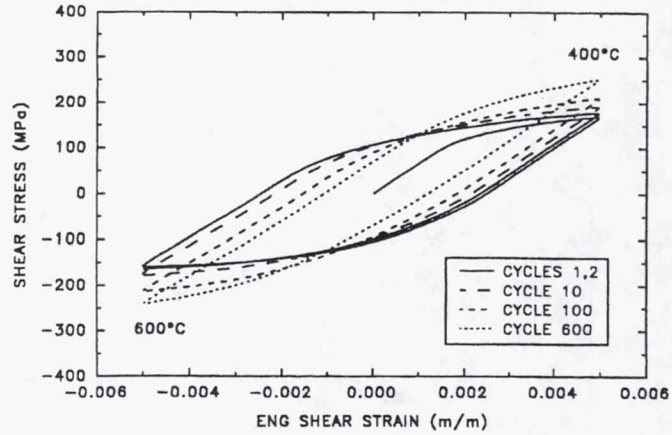

(b) Out-of-phase.

Figure 8.—Stress-strain loops during torsional TMD tests in the 400-600 °C temperature range.

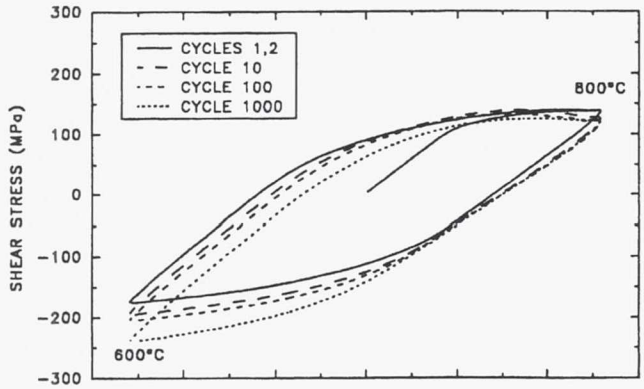

(a) In-phase.

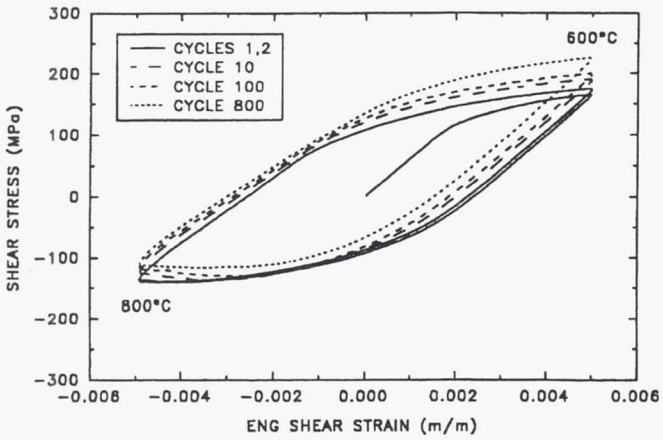

(b) Out-of-phase.

Figure 9.—Stress-strain loops during torsional TMD tests in the 600-800 °C temperature range.

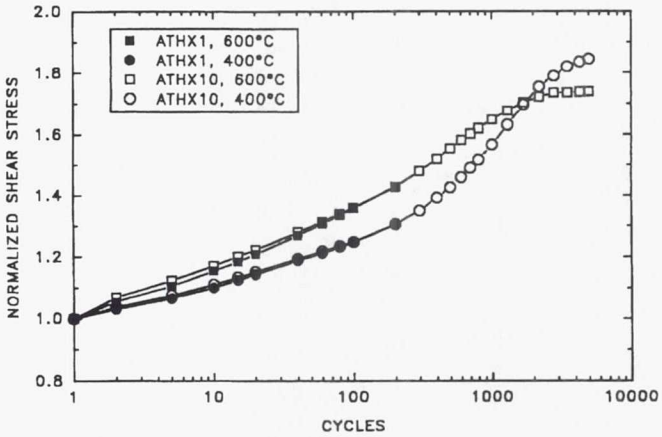

Figure 10.—Comparison of hardening in two in-phase torsional TMD tests with the 400-600 °C temperature range.

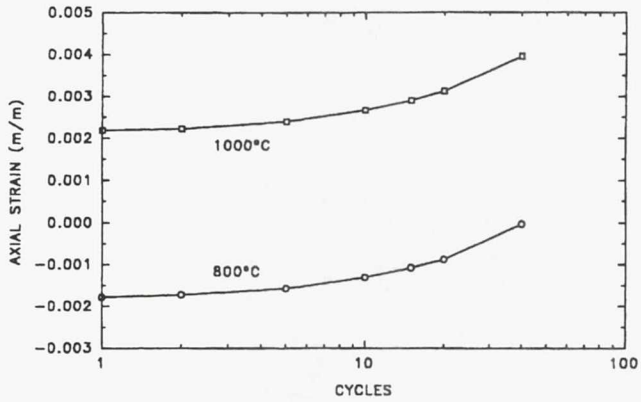

(a) 800-1000 °C, in-phase.

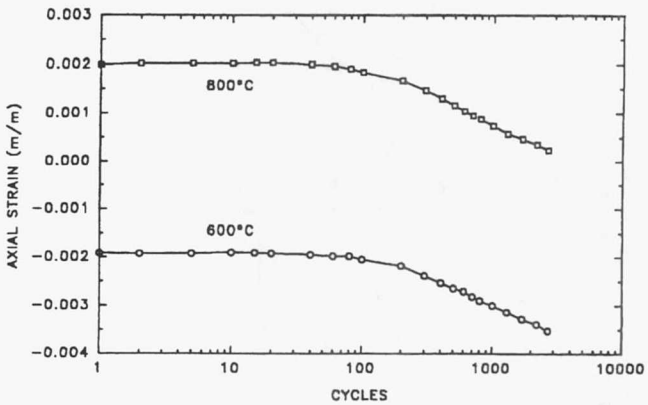

(b) 600-800 °C, in-phase.

Figure 11.—Examples of axial strain ratchetting in torsional TMD tests.

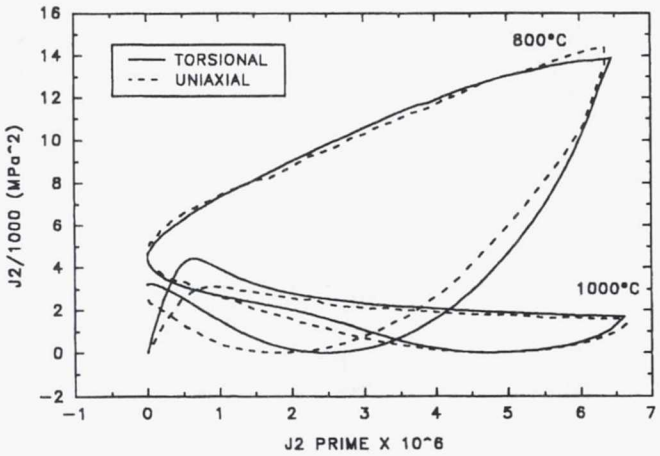

Figure 12.—First cycle J_2'-J_2 loops for torsional and uniaxial tests in 800-1000 °C temperature range: hot/cold temperature sequence.

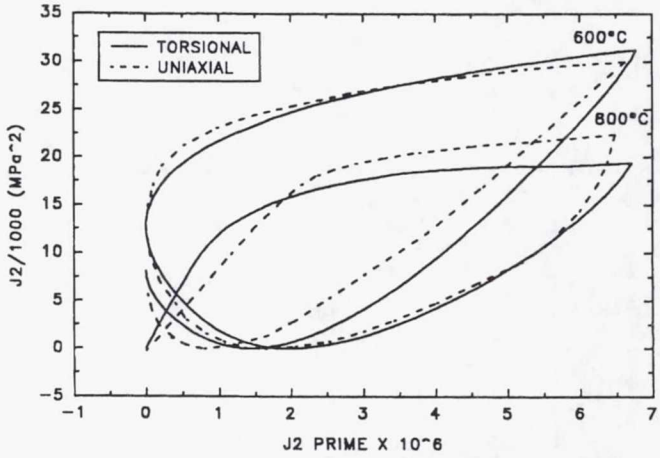

Figure 13.—First cycle J_2'-J_2 loops for torsional and uniaxial tests in 600-800 °C temperature range: hot/cold temperature sequence.

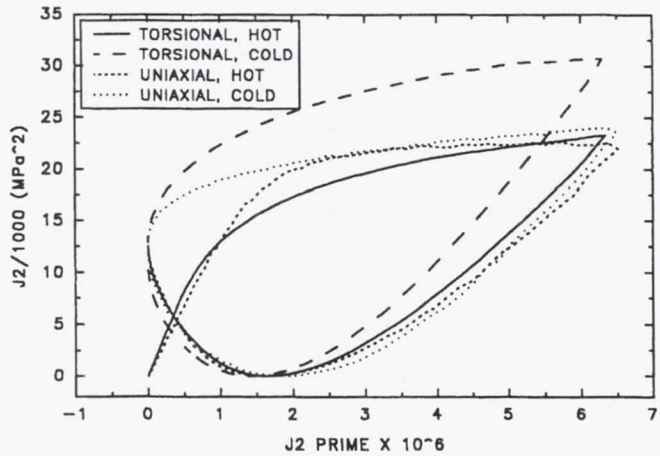

Figure 14.—First cycle J_2'-J_2 loops for torsional and uniaxial tests in 400-600 °C temperature range: hot/cold temperature sequence.

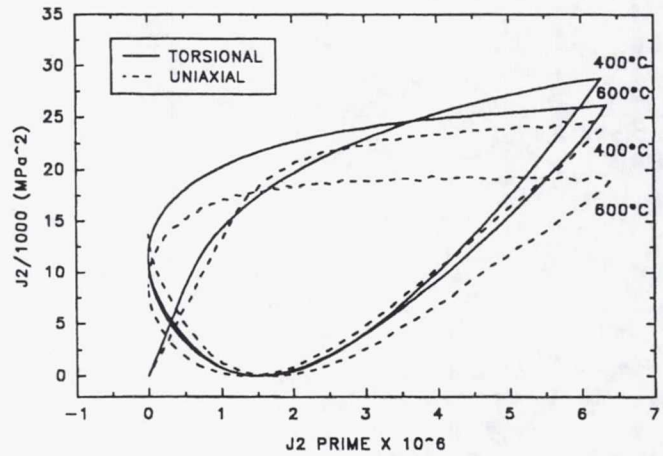

Figure 15.—First cycle J_2'-J_2 loops for torsional and uniaxial tests in 400-600 °C temperature range: cold/hot temperature sequence.

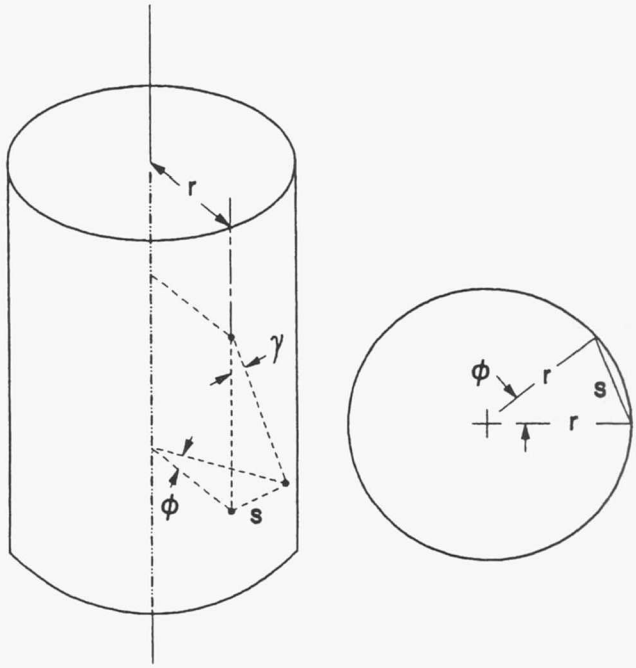

(a) Oblique View (b) Top View

Figure A1.—Geometric parameters established for shear strain calculations in a thin-walled tube.

REPORT DOCUMENTATION PAGE

Form Approved
OMB No. 0704-0188

1. AGENCY USE ONLY (*Leave blank*)	2. REPORT DATE	3. REPORT TYPE AND DATES COVERED
	November 1992	Technical Memorandum

4. TITLE AND SUBTITLE

Experimental Investigation of Cyclic Thermomechanical Deformation in Torsion

5. FUNDING NUMBERS

WU-510-01-50

6. AUTHOR(S)

Michael G. Castelli, Charles E. Bakis, and John R. Ellis

7. PERFORMING ORGANIZATION NAME(S) AND ADDRESS(ES)

Sverdrup Technology, Inc.
Lewis Research Center Group
2001 Aerospace Parkway
Brook Park, Ohio 44142

8. PERFORMING ORGANIZATION REPORT NUMBER

E-7455

9. SPONSORING/MONITORING AGENCY NAMES(S) AND ADDRESS(ES)

National Aeronautics and Space Administration
Lewis Research Center
Cleveland, Ohio 44135-3191

10. SPONSORING/MONITORING AGENCY REPORT NUMBER

NASA TM-105938

11. SUPPLEMENTARY NOTES

Michael G. Castelli, Sverdrup Technology, Inc., Lewis Research Center Group, 2001 Aerospace Parkway, Brook Park, Ohio 44141; Charles E. Bakis, Department of Engineering Science and Mechanics, The Pennsylvania State University, 227 Hammond Building, University Park, Pennsylvania 16802; and John R. Ellis, NASA Lewis Research Center. Responsible person, Michael G. Castelli, (216) 433-8464.

12a. DISTRIBUTION/AVAILABILITY STATEMENT

Unclassified - Unlimited
Subject Category 39

12b. DISTRIBUTION CODE

13. ABSTRACT ***(Maximum 200 words)***

An investigation of thermomechanical testing and deformation behavior of tubular specimens under torsional loading is described. Experimental issues concerning test accuracy and control specific to thermomechanical loadings under a torsional regime are discussed. A series of shear strain-controlled tests involving the nickel-base superalloy Hastelloy X were performed with various temperature excursions and compared to similar thermomechanical uniaxial tests. The concept and use of second invariants of the deviatoric stress and strain tensors as a means of comparing uniaxial and torsional deformations is presented and critiqued for its applicability to the present data. The hardening behavior of the torsional specimens is also briefly presented and discussed in light of previous thermomechanical tests conducted under uniaxial conditions.

14. SUBJECT TERMS

Thermomechanical testing; Deformation; Torsion; Hastelloy X; Deviatoric invariants; Elevated temperature

15. NUMBER OF PAGES

28

16. PRICE CODE

A03

17. SECURITY CLASSIFICATION OF REPORT	18. SECURITY CLASSIFICATION OF THIS PAGE	19. SECURITY CLASSIFICATION OF ABSTRACT	20. LIMITATION OF ABSTRACT
Unclassified	Unclassified	Unclassified	